

Efficient Spatially Sparse Inference for Conditional GANs and Diffusion Models

Muyang Li¹ Ji Lin² Chenlin Meng³ Stefano Ermon³ Song Han² Jun-Yan Zhu¹

¹Carnegie Mellon University ²Massachusetts Institute of Technology ³Stanford University

Abstract

During image editing, existing deep generative models tend to re-synthesize the entire output from scratch, including the unedited regions. This leads to a significant waste of computation, especially for minor editing operations. In this work, we present Spatially Sparse Inference (SSI), a general-purpose technique that selectively performs computation for edited regions and accelerates various generative models, including both conditional GANs and diffusion models. Our key observation is that users tend to make gradual changes to the input image. This motivates us to cache and reuse the feature maps of the original image. Given an edited image, we sparsely apply the convolutional filters to the edited regions while reusing the cached features for the unedited regions. Based on our algorithm, we further propose Sparse Incremental Generative Engine (SIGE) to convert the computation reduction to latency reduction on off-the-shelf hardware. With 1.2%-area edited regions, our method reduces the computation of DDIM by $7.5\times$ and GauGAN by $18\times$ while preserving the visual fidelity. With SIGE, we accelerate the inference time of DDIM by $3.0\times$ on RTX 3090 and $6.6\times$ on Apple M1 Pro CPU, and GauGAN by $4.2\times$ on RTX 3090 and $14\times$ on Apple M1 Pro CPU.

1 Introduction

Deep generative models, such as GANs [1, 2] and diffusion models [3, 4, 5], excel at synthesizing photo-realistic images, enabling many image synthesis and editing applications. For example, users can edit an image by drawing sketches [6, 7], semantic maps [6, 8], or strokes [9]. All of these applications require users to interact with generative models frequently and therefore demand short inference time.

In practice, content creators often edit images gradually and only update a small image region each time. However, even for a minor edit, recent generative models often synthesize the entire image, including the unchanged regions, which leads to a significant waste of computation. As a concrete example shown in Figure 2(a), the result of the previous edits has already been computed, and the user further edits 9.4% area. However, the vanilla DDIM [5] needs to generate the entire image to obtain the newly edited regions, wasting 80% computation on the unchanged regions. A naive approach to address this issue would be to first segment the newly edited regions, synthesize the corresponding output regions, and blend the outputs back into the previous output. Unfortunately, this method often creates visible seams between the newly edited and unedited regions. How could we save the computation by only updating the edited regions without losing global coherence?

In this work, we propose Spatially Sparse Inference (SSI), a general method to accelerate deep generative models, including conditional GANs and diffusion models, by utilizing the spatial sparsity of edited regions. Our method is motivated by the observation that feature maps at the unedited regions remain mostly the same during user editing. As shown in Figure 2(b), our key idea is to reuse the cached feature maps of the previous edits and sparsely update the newly edited regions. Specifically, given user input, we first compute a difference mask to locate the newly edited regions. For each

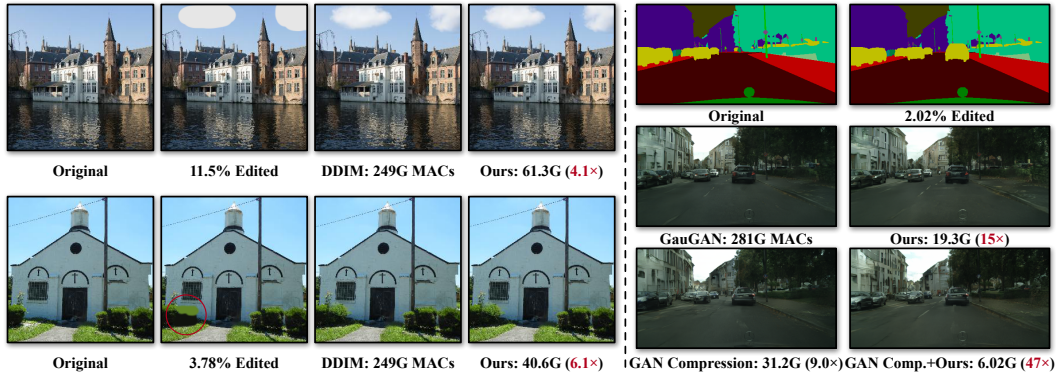


Figure 1: We introduce *Spatially Sparse Inference*, a general-purpose method to selectively perform computations at the edited regions for image editing applications. Our method reduces the computation of DDIM [5] by $4 \sim 6\times$ and GauGAN [8] by $15\times$ for the examples shown in the figures while preserving the image quality. When combined with existing model compression methods such as GAN Compression [10], our method further reduces the computation of GauGAN by $47\times$.

convolution layer in the model, we only apply the filters to the masked regions sparsely while reusing the previous activations for the unchanged regions. The sparse update can significantly reduce the computation without hurting the image quality. However, the sparse update involves a gather-scatter process, which often incurs significant latency overheads for existing deep learning frameworks. To address the issue, we propose *Sparse Incremental Generative Engine (SIGE)* to translate the theoretical computation reduction of our algorithm to measured latency reduction on various hardware.

To evaluate our method, we automatically create new image editing benchmark datasets on LSUN Church [11] and Cityscapes [12]. Without loss of visual fidelity, we reduce the computation of DDIM [5] by $7.5\times$, Progressive Distillation [13] by $2.7\times$, and GauGAN by $18\times$ measured by MACs*. Compared to existing generative model acceleration methods [10, 14, 15, 16, 17, 18, 19], our method directly uses the off-the-shelf pre-trained weights and could be applied to these methods as a plugin. When applied to GAN Compression [10], our method reduces the computation of GauGAN by $\sim 50\times$. See Figure 1 for some examples of our method. With SIGE, we accelerate DDIM $3.0\times$ on RTX 3090 GPU and $6.6\times$ on Apple M1 Pro CPU, and GauGAN $4.2\times$ on RTX 3090 GPU and $38\times$ on Apple M1 Pro CPU. Our code and benchmarks are available at <https://github.com/lmxyy/sige>.

2 Related Work

Generative models. Generative models such as GANs [1, 2, 20, 21], diffusion models [4, 3, 22], and auto-regressive models [23, 24] have demonstrated impressive photorealistic synthesis capability. They have also been extended to conditional image synthesis tasks such as image-to-image translation [25, 6, 26, 27], controllable image generation [9, 28, 8], and real image editing [29, 28, 30, 31, 32, 33, 34, 27]. Unfortunately, recent generative models have become increasingly computationally intensive, compared to their recognition counterparts. For example, GauGAN [8] consumes 281G MACs, $500\times$ more than MobileNet [35, 36, 37]. Similarly, one key limitation of diffusion models [4] is their long inference time and substantial computation cost. To generate one image, DDPM requires hundreds or thousands of forwarding steps [4, 22], which is often infeasible in real-world interactive settings. To improve the sampling efficiency of DDPMs, recent works [5, 38, 39] propose to interpret the sampling process of DDPMs from the perspective of ordinary differential equations. However, these approaches still require hundreds of steps to generate high-quality samples. To further reduce the sampling cost, DDGAN [40] uses a multimodal conditional GAN to model each denoising step. Salimans *et al.* [13] propose to progressively distill a pre-trained DDPM model into a new model that requires fewer steps. Although this approach drastically reduces the sampling steps, the distilled model itself remains computationally prohibitive. Unlike prior work, our work focuses on reducing the computation cost of a pre-trained model. It is complementary to recent efforts on model compression, distillation, and the sampling step reduction of the diffusion models.

Model acceleration. People apply model compression techniques, including pruning [41, 42, 43, 44, 45, 46] and quantization [41, 47, 48, 49, 50, 51], to reduce the computation and model size of off-the-shelf deep learning models. Recent works apply Neural Architecture Search (NAS) [52, 53, 54, 55,

*We measure the computational cost with the number of Multiply-Accumulate operations (MACs). 1 MAC=2 FLOPs.

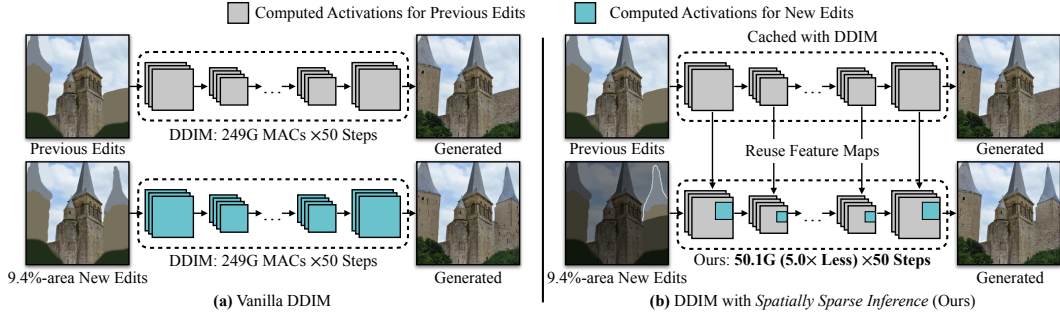


Figure 2: In the interactive editing scenario, a user adds a new building, which occupies 9.4% pixels. **(a)** Vanilla DDIM has to regenerate the *entire* image, even though only 9.4% area is edited. **(b)** Our method instead *reuses* the feature maps of the previous edits and only applies convolutions to the *newly edited* regions sparsely, which has a $5.0\times$ MACs reduction in this case.

[56, 57, 58] to automatically design efficient neural architectures. The above ideas can be successfully applied to accelerate the inference of GANs [10, 59, 60, 61, 14, 62, 15, 16, 17, 18, 19, 63]. Although these methods have achieved prominent compression and speedup ratios, they all reduce the computation from the model dimension but fail to exploit the redundancy in the spatial dimension during image editing. Besides, these methods require re-training the compressed model to maintain performance, while our method can be directly applied to existing pre-trained models. We show that our method can be combined with model compression [10] to achieve a $\sim 50\times$ MACs reduction in Section 4.1.

Sparse computation. Sparse computation has been widely explored in the weight domain [64, 65, 66, 67], input domain [68, 69], and activation domain [70, 71, 72, 73]. For activation sparsity, RRN [74] utilizes the sparsity in the consecutive video frame difference to accelerate video models. However, their sparsity is unstructured, which requires special hardware to reach its full speedup potential. Several works instead use structured sparsity. Li *et al.* [75] use a deep layer cascade to apply more convolutions on the hard regions than the easy regions to improve the accuracy and speed of semantic segmentation. To accelerate 3D object detection, SBNNet [70] uses a spatial mask, either from a priori problem knowledge or an auxiliary network, to sparsify the activations. It adopts a tiling-based sparse convolution algorithm to handle spatial sparsity. Recent works further integrate the spatial mask generation network into the sparse inference network in an end-to-end manner [76] and extend the idea to different tasks [77, 78, 79, 80]. Compared to SBNNet [70], our mask is directly derived from the difference between the original image and the edited image. Additionally, our method does not require any auxiliary network or extra model training. We also introduce other optimizations, such as normalization removal and kernel fusions, to better adapt our engine for image editing.

3 Method

We build our method based on the following observation: during interactive image editing, a user often only changes the image content gradually. As a result, only a small subset of pixels in a local region is being updated at any moment. Therefore, we can reuse the activations of the original image for the unedited regions. As shown in Figure 3, we first pre-compute all activations of the original input image. During the editing process, we locate the edited regions by computing a difference mask between the original and edited image. We then reuse the pre-computed activations for the unedited regions and only update the edited regions by applying convolutional filters to them. In Section 3.1, we show the sparsity in the intermediate activations and present our main algorithm. In Section 3.2, we discuss the technical details of how our Sparse Incremental Generative Engine (SIGE) supports the sparse inference and converts the theoretical computation reduction to measured speedup on hardware.

3.1 Activation Sparsity

Preliminary. First, we closely study the computation within a single layer. We denote A_l^{original} and A_l^{edited} as the input tensor of the original image and edited image to the l -th convolution layer F_l , respectively. W_l and b_l are the weight and bias of F_l . The output of F_l with input A_l^{edited} could be

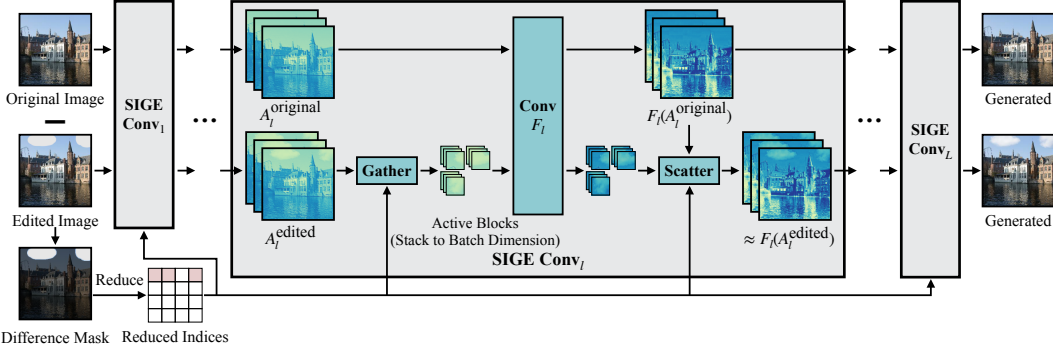


Figure 3: Tiling-based sparse convolution overview. For each convolution F_l in the network, we wrap it into SIGE Conv_l . The activations of the original image are already pre-computed. When getting the edited image, we first compute a difference mask between the original and edited image and reduce the mask to the active block indices to locate the edited regions. In each SIGE Conv_l , we directly gather the active blocks from the edited activation A_l^{edited} according to the reduced indices, stack the blocks along the batch dimension, and feed them into F_l . The gathered blocks have an overlap of width 2 if F_l is 3×3 convolution [70]. After getting the output blocks from F_l , we scatter them back into $F_l(A_l^{\text{original}})$ to get the edited output, which approximates $F_l(A_l^{\text{edited}})$.

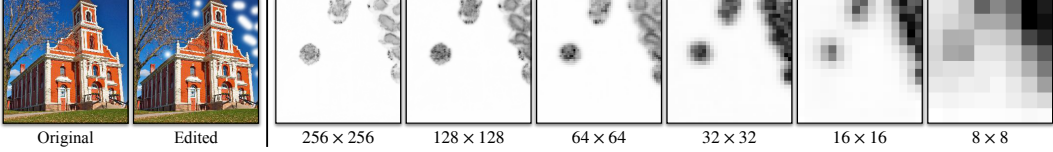


Figure 4: Left: Detailed edit example. Right: Channel-wise average of $|\Delta A_l|$ at the l -th layer of DDIM with different feature map resolutions. $|\Delta A_l|$ is sparse and non-zero values are aggregated at the edited regions.

computed in the following way due to the linearity of convolution:

$$\begin{aligned}
 F_l(A_l^{\text{edited}}) &= W_l * A_l^{\text{edited}} + b_l \\
 &= W_l * (A_l^{\text{edited}} - A_l^{\text{original}}) + (W_l * A_l^{\text{original}} + b_l) \\
 &= W_l * \underbrace{\Delta A_l}_{\text{sparse}} + \underbrace{F_l(A_l^{\text{original}})}_{\text{pre-computed}},
 \end{aligned}$$

where $*$ is the convolution operator and $\Delta A_l = A_l^{\text{edited}} - A_l^{\text{original}}$. If we already pre-computed all the $F_l(A_l^{\text{original}})$, we only need to compute $W_l * \Delta A_l$. Naïvely, computing $W_l * \Delta A_l$ has the same complexity as $W_l * A_l^{\text{edited}}$. However, since the edited image shares similar features with the original image given a small edit, ΔA_l should be sparse. Below, we discuss different strategies to leverage the activation sparsity to accelerate model inference.

Our first attempt was to prune ΔA_l by zeroing out elements smaller than a certain threshold to achieve the target sparsity. Unfortunately, this pruning method fails to achieve measured speedup due to the overheads of the on-the-fly pruning and irregular sparsity pattern.

Structured sparsity. Fortunately, user edits are often highly structured and localized. As a result, ΔA_l should also share the *structured spatial sparsity*, where non-zero values are mostly aggregated within the edited regions, as shown in Figure 4. We then directly use the original image and edited image to compute a difference mask and sparsify ΔA_l with this mask.

3.2 Sparse Engine SIGE

But how could we leverage the structured sparsity to accelerate $W_l * \Delta A_l$? A naïve approach is to crop a rectangular edited region out of ΔA_l for each convolution and only compute features for the cropped regions. Unfortunately, this naïve cropping method works poorly for the irregular edited regions (e.g., the example shown in Figure 4).

Tiling-based sparse convolution. Instead, as shown in Figure 5(a), we use a tiling-based sparse convolution algorithm. We first downsample the difference mask to different scales and dilate the downsampled masks (width 1 for diffusion models and 2 for GauGAN). Then we divide ΔA_l into multiple small blocks of the same size spatially and index the difference mask at the corresponding

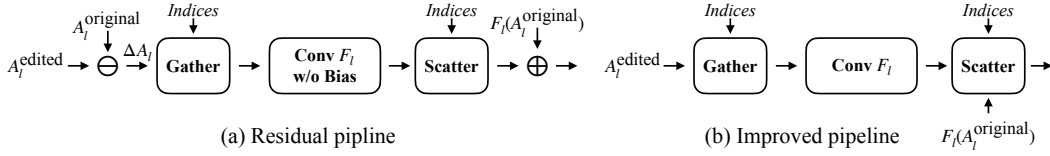


Figure 5: The titling-based sparse convolution pipelines. (a) We first compute the activation difference ΔA_l and gather the active blocks along the batch dimension from it according to the indices reduced from the difference mask. We then feed the blocks into the convolution F_l without bias, scatter the output into a zero tensor, and add the residual $F_l(A_l^{\text{original}})$ back. (b) We directly gather the blocks from A_l^{edited} without computing ΔA_l . F_l is computed with bias. We scatter the output into $F_l(A_l^{\text{original}})$ instead of a zero tensor.

resolution. Each block index refers to a single block with non-zero elements. We then gather the non-zero blocks (we also call them *active blocks*) accordingly along the batch dimension and feed them into the convolution F_l . Finally, we scatter the output blocks into a zero tensor according to the indices to recover the original spatial size and add the pre-computed residual $F_l(A_l^{\text{original}})$ back. The gathered active blocks have an overlap with width 2 for 3×3 convolution to ensure the output blocks of the adjacent input blocks are seamlessly stitched together [70].

This pipeline in Figure 5(a) is equivalent to a simpler pipeline in Figure 5(b). Instead of gathering ΔA_l , we could directly gather A_l^{edited} . The convolution needs to be computed with bias b_l . Besides, we need to scatter the output blocks into $F_l(A_l^{\text{original}})$ instead of a zero tensor. Thus, we do not need to store A_l^{original} anymore, which further saves memory and removes the overheads of addition and subtraction. Figure 3 visualizes the pipeline.

However, the aforementioned pipeline still fails to produce a noticeable speedup due to extra kernel calls and memory movement overheads in Gather and Scatter. For example, the original dense 3×3 convolution with 128 channels and input resolution 256×256 would take 0.78ms on RTX 3090. The sparse convolution using pipeline Figure 5(b) on the example shown in Figure 4 (15.5% edited regions) needs 0.42ms in total, while Gather and Scatter introduce a significant overhead (0.17ms, about 41%). To reduce it, we further optimize SIGE by pre-computing normalization parameters and applying kernel fusion.

Pre-computing normalization parameters. For batch normalization [81], it is easy to remove the normalization layer during inference time since we can use pre-computed mean and variance statistics from model training. However, recent deep generative models often use instance normalization [82, 83] or group normalization [84, 85], which compute the statistics on the fly during inference. These normalization layers incur overheads as we need to estimate the statistics from the full-size tensors. However, as the original and edited images are quite similar given a small user edit, we assume $A_l^{\text{original}} \approx A_l^{\text{edited}}$. This allows us to reuse the statistics of A_l^{original} for the normalization instead of recomputing them for A_l^{edited} . Thus, normalization layers could be replaced by simple Scale+Shift operations with pre-computed A_l^{original} statistics.

Kernel fusion. As mentioned before, both the Gather and Scatter operations introduce significant data movement overheads. To reduce it, we fuse several element-wise operations (Scale+Shift and Nonlinearity) into Gather and Scatter [70, 86, 87] and only apply these element-wise operations to the active blocks (*i.e.*, edited regions). Furthermore, we perform in-place computation to reduce the number of kernel calls and memory allocation overheads.

In Scatter, we need to copy the pre-computed activation $F_l(A_l^{\text{original}})$. This copying operation is highly redundant, as most elements from $F_l(A_l^{\text{original}})$ do not involve any computation given a small edit and will be discarded in the next Gather. To reduce the tensor copying overheads, we fuse the Scatter with the following Gather by directly gathering the active blocks from $F_l(A_l^{\text{original}})$ and the input blocks to be scattered. Sometimes, the residual connection in the ResBlock [88] contains shortcut 1×1 convolution to match the channel number of the residual and the ResBlock output. We also fuse the Scatter in the shortcut branch, main branch, and the residual addition together to avoid the tensor copying overheads in the shortcut Scatter. Please refer to Appendix A for more details.

4 Experiments

Below we first describe our models, baselines, datasets, and evaluation protocols. We then discuss our main qualitative and quantitative results. Finally, we include a detailed ablation study regarding the importance of each algorithmic design.

Models. We conduct experiments on three models, including diffusion models and GAN-based models, to explore the generality of our method.

- *DDIM* [5] is a fast sampling approach for diffusion models. It proposes to interpret the sampling process of diffusion models through the lens of ordinary differential equations.
- *Progressive Distillation (PD)* [13] adopts network distillation [89] to progressively reduce the number of steps for diffusion models.
- *GauGAN* [8] is a paired image-to-image translation model which learns to generate a high-fidelity image given a semantic label map.

Baselines. We compare our methods against the following baselines:

- *Patch.* We crop the smallest patch covering all the edited regions, feed it into the model, and blend the output patch into the original image.
- *Crop.* For each convolution F_l , we crop the smallest rectangular region that covers all masked elements of the activation A_l^{edited} , feed it into F_l , and scatter the output patch into $F_l(A_l^{\text{original}})$.
- *40% Pruning.* We uniformly prune 40% weights of the models without further fine-tuning, as our method directly uses the pre-trained weights. Since the fine-grained pruning is unstructured, it requires special hardware to achieve measured speedup, so we do not report MACs for this baseline.
- *0.19 GauGAN.* We reduce each convolution layer of GauGAN to 19% channels ($21 \times$ MACs reduction) and train it from scratch.
- *GAN Compression* [10]. A general-purpose compression method for conditional GANs. *GAN Comp. (S)* means GAN Compression with a larger compression ratio.
- *0.5 Original* means linearly scaling each layer of the original model to 50% channels, and we only use this to benchmark our efficiency results.

Datasets. We use the following two datasets in our experiments:

- *LSUN Church.* We use the LSUN Church Outdoor dataset [11] and follow the same preprocessing steps as prior works [4, 38]. To automatically generate a stroke editing benchmark, we first use Detic [90] to segment the images in the validation set. For each segmented object, we use its segmentation mask to inpaint the image by CoModGAN [91] and treat the inpainted image as the original image. We generate the corresponding user strokes by first blurring the masked regions with the median filter and quantizing it into 6 colors following SEdit [9]. We collect 454 editing pairs in total (431 synthetic + 23 manual). We evaluate DDIM [5] and PD [13] on this dataset.
- *Cityscapes.* The dataset [12] contains images of German street scenes. The training and validation sets consist of 2975 and 500 images, respectively. Our editing dataset has 1505 editing pairs in total. We evaluate GauGAN [8] on this dataset.

Please refer to Appendix B for more details about the benchmark datasets.

Metrics. Following previous works [9, 10, 8], we use the standard metrics Peak Signal Noise Ratio (PSNR, higher is better), LPIPS (lower is better) [92], and Fréchet Inception Distance (FID, lower is better) [93, 94][†] to evaluate the image quality on both LSUN Church [11] and Cityscapes [12]. For Cityscapes, we adopt a semantic segmentation metric to evaluate the generated images. Specifically, we run DRN-D-105 [95] on the generated images and compute the mean Intersection over Union (mIoU) of the segmentation results. Generally, a higher mIoU indicates that the generated images look more realistic and better align to the input.

[†]We use **clean-fid** for FID calculation.

Model	Method	MACs		PSNR (\uparrow)		LPIPS (\downarrow)		FID (\downarrow)	mIoU (\uparrow)
		Value	Ratio	with G.T.	with Orig.	with G.T.	with Orig.		
DDIM	Original	249G	–	26.8	–	0.069	–	65.4	–
	40% Pruning	–	–	24.9	31.0	0.991	0.101	72.2	–
	Patch	72.0G	3.5 \times	26.8	40.6	0.076	0.022	66.4	–
	Ours	65.3G	3.8\times	26.8	52.4	0.070	0.009	65.8	–
PD	Original	66.9G	–	21.9	–	0.143	–	90.0	–
	40% Pruning	–	–	21.6	37.6	0.164	0.051	101	–
	Ours	32.5G	2.1\times	21.9	60.7	0.154	0.003	90.1	–
GauGAN	Original	281G	–	15.8	–	0.409	–	55.4	62.4
	GAN Comp. [10]	31.2G	9.0 \times	15.8	19.5	0.412	0.288	55.5	61.5
	Ours	30.7G	9.2\times	15.8	26.5	0.413	0.113	54.4	62.1
	0.19 GauGAN	13.3G	21 \times	15.5	18.6	0.424	0.322	57.9	53.5
	GAN Comp. (S)	9.64G	29 \times	15.7	19.1	0.422	0.310	50.4	57.4
	GAN Comp.+Ours	7.06G	40\times	15.7	19.2	0.416	0.299	54.6	60.0

Table 1: Quantitative quality evaluation. PSNR/LPIPS *with G.T.* means computing the metrics with the ground-truth images, and *with Orig.* means computing with the generated samples from the original model. *40% Pruning*: Uniformly pruning 40% weights of the model without fine-tuning. *Patch*: Cropping the smallest image patch that covers all the edited region and blending the output patch into the original image. *0.19 GauGAN*: Uniformly reducing each layer of GauGAN to 19% channels and training from scratch. *GAN Comp. (S)*: GAN Compression with a larger compression ratio. For all models, our method outperforms other baselines with less computation. When applying our method to GAN Compression, we reduce the MACs of GauGAN by 40 \times with minor performance degradation.

Implementation details. The number of denoising steps for DDIM and PD are 100 and 8, respectively, and we use 50 and 5 steps for SDEdit. We dilate the difference mask by 5, 2, 5, and 1 pixels for DDIM, PD with resolution 128, PD with resolution 256 and GauGAN, respectively. Besides, we apply our sparse kernel to all convolution layers whose input feature map resolutions are larger than 32×32 , 16×16 , 8×16 and 16×32 for DDIM, PD, original GauGAN and GAN Compression, respectively. For DDIM [5] and PD [13], we pre-compute and reuse the statistics of the original image for all group normalization layers [84]. For GAN Compression [10], we pre-compute and reuse the statistics of the original image for all instance normalization layers [82] whose resolution is higher than 16×32 . For all models, the sparse block size for 3×3 convolution is 6 and 1×1 convolution is 4.

4.1 Main Results

Image quality. We report the quantitative results of applying our method on DDIM [5], Progressive Distillation (PD) [13], and GauGAN [8] in Table 1 and show the qualitative results in Figure 6. For PSNR and LPIPS, *with G.T.* means computing the metric with the ground-truth images. *With Orig.* means computing the metric with the samples generated by the original model. On LSUN Church, we only use 431 synthetic images for the *PSNR/LPIPS with G.T.* metrics, as manual edits do not have ground truths. For the other metrics, we use the entire LSUN Church dataset (431 synthetic + 23 manual). On Cityscapes, we view the synthetic semantic maps as the original input and the ground-truth semantic maps as the edited input for the *PSNR/LPIPS with G.T.* metrics, which has 1505 samples. For the other metrics, we include the symmetric edits (view the ground-truth semantic maps as the original inputs and synthetic semantic maps as the edited inputs), which has 3010 samples in total. For the models with method *Patch* and *Ours*, whose computation is edit-dependent, we measure the average MACs over the whole dataset.

For DDIM and Progressive Distillation, our method outperforms all baselines consistently and achieves results on par with the original model. The *Patch* inference fails when the edited region is small as the global context is insufficient. Although our method only applies convolutional filters to the local edited regions, we could reuse the global context stored in the original activations. Therefore, our method could perform the same as the original model. For GauGAN, our method also performs better than GAN Compression [10] with an even larger MACs reduction. When applying our method to GAN Compression, we further achieve a $\sim 40\times$ MACs reduction with minor performance degradation, beating both *0.19 GauGAN* and *GAN Comp. (S)*.

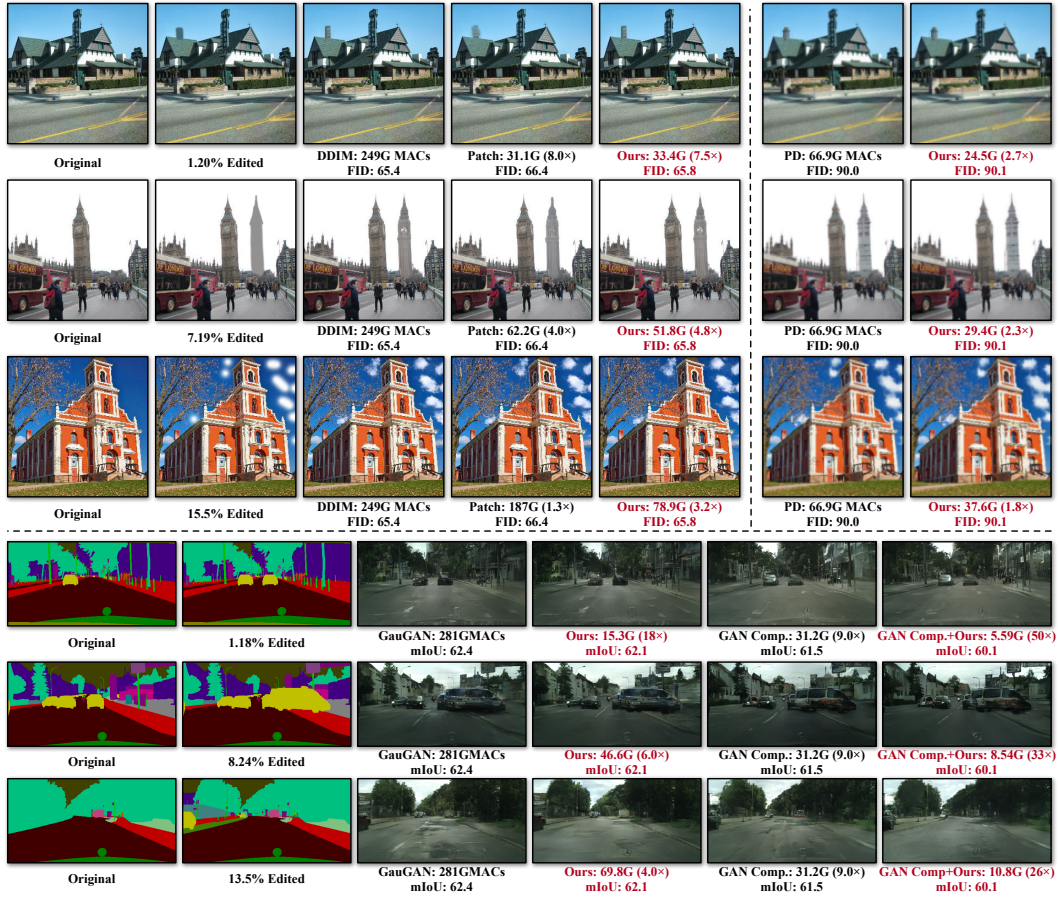


Figure 6: Qualitative results of our method under different edit sizes. Our method well preserves the visual fidelity of the original model without losing global context. On the contrary, *Patch* (cropping the smallest image patch that covers all the edited regions and scattering the output patch back into the original image) performs poorly because of the lack of global context when the edit is small.

Model efficiency. For real-world interactive image editing applications, inference acceleration on hardware is more critical than the computation reduction. To verify the effectiveness of our proposed engine, we measure the speedup of the edit examples shown in Figure 6 on four devices, including NVIDIA RTX 3090, NVIDIA RTX 2080Ti, Intel Core i9-10920X CPU, and Apple M1 Pro CPU, with different computational powers. We use batch size 1 to simulate real-world use. For GPU devices, we first perform 200 warm-up runs and measure the average latency of the next 200 runs. For CPU devices, we perform 10 warm-up runs and 10 test runs, repeat this process 5 times and report the average latency. The latency is measured in PyTorch 1.7[‡]. The results are shown in Table 2.

The original Progressive Distillation [13] can only generate 128×128 images, which is too small for real use. We add some extra layers to adapt the model to resolution 256×256 . For fair comparisons, we also pre-compute the normalization parameters for the *Crop* baseline. When the edit pattern is like a rectangle, this baseline reduces similar computation with ours (*e.g.*, the first example of DDIM in Figure 6). However, the speedup is still worse than ours on RTX 3090, 2080Ti and Intel Core i9-10920X due to the large memory index overheads in native PyTorch. When the edited region is far from a rectangle (*e.g.*, the third example of DDIM), the cropped patches have much redundancy. Therefore, even though only 15.5% region is edited, the MACs reduction is only $1.6\times$. With 1.2% edit size, our method achieves a $7.5\times$, $4.6\times$, and $18\times$ MACs reduction for DDIM, Progressive Distillation, and GauGAN, respectively. With SIGE, we achieve at most $4.1\times$, $2.9\times$, $6.0\times$ and $14\times$ speedup on RTX 3090, 2080Ti, Intel Core i9-10920X and Apple M1 Pro CPU, respectively. When applied to GAN Compression, SIGE achieves a $9.5\times$ and $38\times$ latency reduction on Intel Core i9-10920X and Apple M1 Pro CPU, respectively.

[‡]<https://github.com/pytorch/pytorch>

Model	Edit Size	Method	MACs		3090		2080Ti		Intel Core i9-10920X		Apple M1 Pro	
			Value	Ratio	Value	Ratio	Value	Ratio	Value	Ratio	Value	Ratio
DDIM	-	Original	248G	-	37.5ms	-	54.6ms	-	609ms	-	12.9s	-
		0.5 Original	62.5G	4.0×	20.0ms	1.9×	31.2ms	1.8×	215ms	2.8×	3.22s	4.0×
	1.20%	Crop	32.6G	7.6×	15.5ms	2.4×	29.3ms	1.9×	185ms	3.3×	1.85s	6.9×
		Ours	33.4G	7.5×	12.6ms	3.0×	19.1ms	2.9×	147ms	4.1×	1.96s	6.6×
	15.5%	Crop	155G	1.6×	30.5ms	1.2×	44.5ms	1.2×	441ms	1.4×	8.09s	1.6×
		Ours	78.9G	3.2×	19.4ms	1.9×	29.8ms	1.8×	304ms	2.0×	5.04s	2.6×
PD256	-	Original	119G	-	35.1ms	-	51.2ms	-	388ms	-	6.18s	-
		0.5 Original	31.0G	3.8×	29.4ms	1.2×	43.2ms	1.2×	186ms	2.1×	1.72s	3.6×
	1.20%	Ours	25.9G	4.6×	18.6ms	1.9×	26.4ms	1.9×	152ms	2.5×	1.55s	4.0×
	15.5%	Ours	48.5G	2.5×	21.4ms	1.6×	30.7ms	1.7×	250ms	1.6×	3.22s	1.9×
GauGAN	-	Original	281G	-	45.4ms	-	49.5ms	-	682ms	-	14.1s	-
		GAN Compression	31.2G	9.0×	17.0ms	2.7×	25.0ms	2.0×	333ms	2.1×	2.11s	6.7×
	1.18%	Ours	15.3G	18×	11.1ms	4.1×	19.3ms	2.6×	114ms	6.0×	0.990s	14×
		GAN Comp.+Ours	5.59G	50×	10.8ms	4.2×	16.2ms	3.1×	53.1ms	13×	0.370s	38×
	13.5%	Ours	69.8G	4.0×	17.8ms	2.5×	27.1ms	1.8×	238ms	2.9×	4.06s	3.5×
		GAN Comp.+Ours	10.8G	26×	11.8ms	3.8×	17.4ms	2.8×	94.4ms	7.2×	0.741s	19×

Table 2: Measured latency speedup on different devices. The detailed edit examples are shown in Figure 6. *0.5 Original*: Linearly scaling each layer of the model to 50% channels. *Crop*: For each convolution, we find a smallest patch covering the masked elements, crop it out, feed it into the convolution and scatter the output patch into the original image activation. Our method could reduce up to 18× MACs, and achieve up to 4.1×, 2.9×, 6.0× and 14× latency reduction on NVIDIA RTX 3090, 2080Ti, Intel Core i9-10920X and M1 Pro CPU. With GAN Compression, we could further speed up GauGAN by 9.5× on Intel Core-i9 and 38× on Apple M1 Pro CPU.

MACs	Optimizations			Latency	
	Sparse	Norm.	Elem. Sct.	Value	Ratio
249G				54.6ms	-
	✓			34.0ms	1.6×
32.6G	✓	✓		29.6ms	1.8×
(7.6×	✓	✓	✓	20.7ms	2.6×
	✓	✓	✓	19.1ms	2.9×

(a)

Method	Edit Size	MACs		PyTorch		TensorRT	
		Value	Ratio	Value	Ratio	Value	Ratio
Original	-	249G	-	54.6ms	-	47.7ms	-
	1.20%	33.4G	7.5×	19.1ms	2.9×	14.4ms	3.3×
Ours	7.19%	51.8G	4.8×	22.1ms	2.5×	18.6ms	2.6×
	15.5%	78.9G	3.2×	29.8ms	1.8×	26.9ms	1.8×

(b)

Table 3: (a) Ablation study of each kernel optimization. **Sparse**: Using tiling-based sparse convolution. **Norm.**: Pre-computing normalization parameters. **Elem.**: Fusing element-wise operations. **Sct.**: Fusing Scatter to reduce the tensor copying overheads. With all optimizations, we could reduce the latency of DDIM by 2.9× on NVIDIA RTX 2080Ti. (b) Latency comparisons of DDIM on RTX 2080Ti between PyTorch and TensorRT. The speedup ratio is larger in TensorRT than PyTorch, especially when the edit size is small.

4.2 Ablation Study

Below we perform several ablation studies to show the effectiveness of each design choice.

Memory usage. The pre-computed activations of the original image require additional memory storage. We profile the peak memory usage of the original model and our method in PyTorch. Our method only increases the peak memory usage of a single forward for DDIM, PD, GauGAN, and GAN Compression by 0.1G, 0.1G, 0.8G, and 0.3G, respectively. Specifically, it needs to store additional 169M, 56M, 275M, and 120M parameters for DDIM [5], PD [13], original GauGAN [8] and GAN Compression [10], respectively, for a single forward. For the diffusion models, we need to store activations for all iteration steps (*e.g.*, 50 for DDIM and 5 for PD). However, data movement and kernel computation are asynchronous on GPU, so we could store the activations in CPU memory and load the on-demand ones on GPU to reduce peak memory usage.

Speedup of each design. Table 3a shows the effectiveness of each kernel optimization we add to SIGE for DDIM [5] on RTX 2080Ti. Naïvely applying the tiling-based sparse convolution could reduce the computation by 7.6×. Still, the latency reduction is only 1.6× due to the large memory overheads in Gather and Scatter. Pre-computing the normalization parameters could remove the latency of normalization statistics calculation and reduce the overall latency to 29.6ms. Fusing

element-wise operations into the Gather and Scatter could remove some redundant operations that are applied to the unedited regions and also reduce the memory allocation overheads (about 9ms). Finally, fusing the Scatter and Gather to Scatter-Gather and Scatter in the shortcut branch and main branch could further reduce about 1.6ms tensor copying overheads, achieving $2.9\times$ speedup.

Experiments with TensorRT. Real-world model deployment also depends on deep learning backends with optimized libraries and runtimes. To demonstrate the effectiveness and extensibility of SIGE, we also implement our kernels in a widely-used backend TensorRT[§] and benchmark the DDIM latency results on RTX 2080Ti in Table 3b. Specifically, our speedup ratio becomes more prominent with TensorRT compared to PyTorch, especially for small edits, as TensorRT better supports small convolutional kernels with higher GPU utilization than PyTorch.

5 Conclusion & Discussion

For image editing, existing deep generative models often waste computation by re-synthesizing the image regions that do not require modifications. To solve this issue, we have presented a general-purpose method, Spatially Sparse Inference (SSI), to selectively perform computation on edited regions, and Sparse Incremental Generative Engine (SIGE) to convert the computation reduction to latency reduction on commonly-used hardware. We have demonstrated the effectiveness of our approach in various hardware settings.

Limitations. As discussed in Section 4.2, our method requires extra memory to store the original activations, which slightly increases the peak GPU memory usage. It may not work on certain memory-constrained devices, especially for the diffusion models (*e.g.*, DDIM [5]), since our method requires storing activations of all denoising steps.

Our engine has limited speedup on convolution with low resolution. When the input resolution is low, the active block size needs to be even smaller to get a decent sparsity, such as 1 or 2. However, such extremely small block sizes have bad memory locality and will result in low hardware efficiency.

Besides, we sometimes observe noticeable boundary between the edited regions and unedited regions in our generated samples of GauGAN [8]. This is because, for GauGAN model, the unedited region will also change slightly when we perform normal inference. However, since our method does not update the unedited region, there may be some visible seams between the edited and unedited regions, even though the semantic is coherent. Dilating the difference mask would help reduce the gap.

In most cases, the edit will only update the edited regions. However, sometimes the edit will also introduce global illumination changes such as shadow and reflection. For this case, as we only update the edited regions, we cannot update the global changes outside the edited regions accordingly.

Societal impact. In this paper, we investigate how to update user edit locally without losing global coherence to enable smoother interaction with the generative models. In real-world scenarios, people could use an interactive interface to edit an image, and our method could provide a quick and high-quality preview for their edit, which eases the process of visual content creation and reduces energy consumption, leading to a greener AI application. The reduced cost also provides a good user experience for lower-end devices, which further democratize the applications of generative models.

However, our method can be utilized by malicious users to generate fake contents, deceive people, and spread misinformation, which may lead to potential negative social impacts. Following previous works [9], we explicitly specify the usage permission of our engine with proper licenses. Additionally, we run a forensics detector [96] to detect the generated results of our method. On GauGAN, our generated images can be detected with 97.2% average precision (AP). However, on DDIM [5] and Progressive Distillation [13], the APs are only 56.6% and 52.4%. Such low APs are caused by the model differences between GANs and diffusion models, as observed in SDEdit [9]. We believe developing forensic methods for diffusion models is a critical future research direction.

Acknowledgment. We thank Yaoyao Ding, Zihao Ye, Lianmin Zheng, Haotian Tang, and Ligeng Zhu for the helpful comments on the engine design. We also thank George Cazenavette, Kangle Deng, Ruihan Gao, Daohan Lu, Sheng-Yu Wang and Bingliang Zhang for their valuable feedback. The project is partly supported by NSF, MIT-IBM Watson AI Lab, Kwai Inc, and Sony Corporation.

[§]We benchmark the results with TensorRT 8.4.

References

- [1] Ian Goodfellow, Jean Pouget-Abadie, Mehdi Mirza, Bing Xu, David Warde-Farley, Sherjil Ozair, Aaron Courville, and Yoshua Bengio. Generative adversarial nets. *NeurIPS*, 2014. 1, 2
- [2] Tero Karras, Samuli Laine, and Timo Aila. A style-based generator architecture for generative adversarial networks. In *CVPR*, 2019. 1, 2
- [3] Jascha Sohl-Dickstein, Eric Weiss, Niru Maheswaranathan, and Surya Ganguli. Deep unsupervised learning using nonequilibrium thermodynamics. In *ICML*, 2015. 1, 2
- [4] Jonathan Ho, Ajay Jain, and Pieter Abbeel. Denoising diffusion probabilistic models. *NeurIPS*, 2020. 1, 2, 6
- [5] Jiaming Song, Chenlin Meng, and Stefano Ermon. Denoising diffusion implicit models. In *ICLR*, 2020. 1, 2, 6, 7, 9, 10, 15, 17, 18, 19, 21
- [6] Phillip Isola, Jun-Yan Zhu, Tinghui Zhou, and Alexei A Efros. Image-to-image translation with conditional adversarial networks. In *CVPR*, 2017. 1, 2
- [7] Patsorn Sangkloy, Jingwan Lu, Chen Fang, Fisher Yu, and James Hays. Scribbler: Controlling deep image synthesis with sketch and color. In *CVPR*, 2017. 1
- [8] Taesung Park, Ming-Yu Liu, Ting-Chun Wang, and Jun-Yan Zhu. Semantic image synthesis with spatially-adaptive normalization. In *CVPR*, 2019. 1, 2, 6, 7, 9, 10, 17, 19, 22
- [9] Chenlin Meng, Yutong He, Yang Song, Jiaming Song, Jiajun Wu, Jun-Yan Zhu, and Stefano Ermon. SDEdit: Guided image synthesis and editing with stochastic differential equations. In *ICLR*, 2022. 1, 2, 6, 10, 17
- [10] Muyang Li, Ji Lin, Yaoyao Ding, Zhijian Liu, Jun-Yan Zhu, and Song Han. Gan compression: Efficient architectures for interactive conditional gans. In *CVPR*, 2020. 2, 3, 6, 7, 9, 17, 18, 19
- [11] Fisher Yu, Yinda Zhang, Shuran Song, Ari Seff, and Jianxiong Xiao. Lsun: Construction of a large-scale image dataset using deep learning with humans in the loop. *arXiv preprint arXiv:1506.03365*, 2015. 2, 6, 18, 19
- [12] Marius Cordts, Mohamed Omran, Sebastian Ramos, Timo Rehfeld, Markus Enzweiler, Rodrigo Benenson, Uwe Franke, Stefan Roth, and Bernt Schiele. The cityscapes dataset for semantic urban scene understanding. In *CVPR*, 2016. 2, 6, 18, 19
- [13] Tim Salimans and Jonathan Ho. Progressive distillation for fast sampling of diffusion models. In *ICLR*, 2021. 2, 6, 7, 8, 9, 10, 17, 18, 19
- [14] Liang Hou, Zehuan Yuan, Lei Huang, Huawei Shen, Xueqi Cheng, and Changhu Wang. Slimmable generative adversarial networks. In *AAAI*, 2021. 2, 3
- [15] Yonggan Fu, Wuyang Chen, Haotao Wang, Haoran Li, Yingyan Lin, and Zhangyang Wang. Autogan-distiller: Searching to compress generative adversarial networks. In *ICML*, 2020. 2, 3
- [16] Shaojie Li, Mingbao Lin, Yan Wang, Chao Fei, Ling Shao, and Rongrong Ji. Learning efficient gans for image translation via differentiable masks and co-attention distillation. *IEEE Transactions on Multimedia*, 2022. 2, 3
- [17] Qing Jin, Jian Ren, Oliver J Woodford, Jiazhao Wang, Geng Yuan, Yanzhi Wang, and Sergey Tulyakov. Teachers do more than teach: Compressing image-to-image models. In *CVPR*, 2021. 2, 3
- [18] Tamar Rott Shaham, Michaël Gharbi, Richard Zhang, Eli Shechtman, and Tomer Michaeli. Spatially-adaptive pixelwise networks for fast image translation. In *CVPR*, 2021. 2, 3
- [19] Haotao Wang, Shupeng Gui, Haichuan Yang, Ji Liu, and Zhangyang Wang. Gan slimming: All-in-one gan compression by a unified optimization framework. In *ECCV*, 2020. 2, 3
- [20] Tero Karras, Samuli Laine, Miika Aittala, Janne Hellsten, Jaakko Lehtinen, and Timo Aila. Analyzing and improving the image quality of stylegan. In *CVPR*, 2020. 2
- [21] Andrew Brock, Jeff Donahue, and Karen Simonyan. Large scale gan training for high fidelity natural image synthesis. In *ICLR*, 2019. 2
- [22] Prafulla Dhariwal and Alexander Nichol. Diffusion models beat gans on image synthesis. *NeurIPS*, 2021. 2
- [23] Patrick Esser, Robin Rombach, and Bjorn Ommer. Taming transformers for high-resolution image synthesis. In *CVPR*, 2021. 2
- [24] Ali Razavi, Aaron Van den Oord, and Oriol Vinyals. Generating diverse high-fidelity images with vq-vae-2. In *NeurIPS*, volume 32, 2019. 2
- [25] Chitwan Saharia, William Chan, Huiwen Chang, Chris Lee, Jonathan Ho, Tim Salimans, David Fleet, and Mohammad Norouzi. Palette: Image-to-image diffusion models. In *SIGGRAPH*, 2022. 2

- [26] Jun-Yan Zhu, Taesung Park, Phillip Isola, and Alexei A Efros. Unpaired image-to-image translation using cycle-consistent adversarial networks. In *ICCV*, 2017. 2
- [27] Peihao Zhu, Rameen Abdal, Yipeng Qin, and Peter Wonka. Sean: Image synthesis with semantic region-adaptive normalization. In *CVPR*, 2020. 2
- [28] Alex Nichol, Prafulla Dhariwal, Aditya Ramesh, Pranav Shyam, Pamela Mishkin, Bob McGrew, Ilya Sutskever, and Mark Chen. Glide: Towards photorealistic image generation and editing with text-guided diffusion models. *arXiv preprint arXiv:2112.10741*, 2021. 2
- [29] Jooyoung Choi, Sungwon Kim, Yonghyun Jeong, Youngjune Gwon, and Sungroh Yoon. Ilvr: Conditioning method for denoising diffusion probabilistic models. In *ICCV*, 2021. 2
- [30] Gwanghyun Kim and Jong Chul Ye. Diffusionclip: Text-guided image manipulation using diffusion models. *arXiv preprint arXiv:2110.02711*, 2021. 2
- [31] Jun-Yan Zhu, Philipp Krähenbühl, Eli Shechtman, and Alexei A Efros. Generative visual manipulation on the natural image manifold. In *ECCV*, 2016. 2
- [32] Or Patashnik, Zongze Wu, Eli Shechtman, Daniel Cohen-Or, and Dani Lischinski. Styleclip: Text-driven manipulation of stylegan imagery. In *ICCV*, 2021. 2
- [33] Rameen Abdal, Yipeng Qin, and Peter Wonka. Image2stylegan: How to embed images into the stylegan latent space? In *ICCV*, 2019. 2
- [34] Rameen Abdal, Yipeng Qin, and Peter Wonka. Image2stylegan++: How to edit the embedded images? In *CVPR*, 2020. 2
- [35] Andrew Howard, Mark Sandler, Grace Chu, Liang-Chieh Chen, Bo Chen, Mingxing Tan, Weijun Wang, Yukun Zhu, Ruoming Pang, Vijay Vasudevan, et al. Searching for mobilenetv3. In *ICCV*, 2019. 2
- [36] Andrew G Howard, Menglong Zhu, Bo Chen, Dmitry Kalenichenko, Weijun Wang, Tobias Weyand, Marco Andreetto, and Hartwig Adam. Mobilenets: Efficient convolutional neural networks for mobile vision applications. *arXiv preprint arXiv:1704.04861*, 2017. 2
- [37] Mark Sandler, Andrew Howard, Menglong Zhu, Andrey Zhmoginov, and Liang-Chieh Chen. Mobilenetv2: Inverted residuals and linear bottlenecks. In *CVPR*, 2018. 2
- [38] Yang Song, Jascha Sohl-Dickstein, Diederik P Kingma, Abhishek Kumar, Stefano Ermon, and Ben Poole. Score-based generative modeling through stochastic differential equations. In *ICLR*, 2020. 2, 6
- [39] Zhifeng Kong and Wei Ping. On fast sampling of diffusion probabilistic models. In *ICML Workshop on Invertible Neural Networks, Normalizing Flows, and Explicit Likelihood Models*, 2021. 2
- [40] Zhisheng Xiao, Karsten Kreis, and Arash Vahdat. Tackling the generative learning trilemma with denoising diffusion GANs. In *ICLR*, 2022. 2
- [41] Song Han, Huizi Mao, and William J Dally. Deep Compression: Compressing Deep Neural Networks with Pruning, Trained Quantization and Huffman Coding. In *ICLR*, 2016. 2
- [42] Yihui He, Ji Lin, Zhijian Liu, Hanrui Wang, Li-Jia Li, and Song Han. AMC: AutoML for Model Compression and Acceleration on Mobile Devices. In *ECCV*, 2018. 2
- [43] Ji Lin, Yongming Rao, Jiwen Lu, and Jie Zhou. Runtime neural pruning. In *NeurIPS*, 2017. 2
- [44] Yihui He, Xiangyu Zhang, and Jian Sun. Channel pruning for accelerating very deep neural networks. In *ICCV*, 2017. 2
- [45] Zhuang Liu, Jianguo Li, Zhiqiang Shen, Gao Huang, Shoumeng Yan, and Changshui Zhang. Learning efficient convolutional networks through network slimming. In *ICCV*, 2017. 2
- [46] Zechun Liu, Haoyuan Mu, Xiangyu Zhang, Zichao Guo, Xin Yang, Kwang-Ting Cheng, and Jian Sun. MetaPruning: Meta Learning for Automatic Neural Network Channel Pruning. In *ICCV*, 2019. 2
- [47] Shuchang Zhou, Yuxin Wu, Zekun Ni, Xinyu Zhou, He Wen, and Yuheng Zou. Dorefa-net: Training low bitwidth convolutional neural networks with low bitwidth gradients. *arXiv preprint arXiv:1606.06160*, 2016. 2
- [48] Mohammad Rastegari, Vicente Ordonez, Joseph Redmon, and Ali Farhadi. Xnor-net: Imagenet classification using binary convolutional neural networks. In *ECCV*, 2016. 2
- [49] Kuan Wang, Zhijian Liu, Yujun Lin, Ji Lin, and Song Han. Haq: Hardware-aware automated quantization with mixed precision. In *CVPR*, 2019. 2
- [50] Jungwook Choi, Zhuo Wang, Swagath Venkataramani, Pierce I-Jen Chuang, Vijayalakshmi Srinivasan, and Kailash Gopalakrishnan. Pact: Parameterized clipping activation for quantized neural networks. *arXiv preprint arXiv:1805.06085*, 2018. 2
- [51] Benoit Jacob, Skirmantas Kligys, Bo Chen, Menglong Zhu, Matthew Tang, Andrew Howard, Hartwig Adam, and Dmitry Kalenichenko. Quantization and training of neural networks for efficient integer-arithmetic-only inference. In *CVPR*, 2018. 2

- [52] Barret Zoph and Quoc V Le. Neural Architecture Search with Reinforcement Learning. In *ICLR*, 2017. 3
- [53] Barret Zoph, Vijay Vasudevan, Jonathon Shlens, and Quoc V. Le. Learning Transferable Architectures for Scalable Image Recognition. In *CVPR*, 2018. 3
- [54] Haoxiao Liu, Karen Simonyan, and Yiming Yang. DARTS: Differentiable Architecture Search. In *ICLR*, 2019. 3
- [55] Han Cai, Ligeng Zhu, and Song Han. ProxylessNAS: Direct Neural Architecture Search on Target Task and Hardware. In *ICLR*, 2019. 3
- [56] Mingxing Tan, Bo Chen, Ruoming Pang, Vijay Vasudevan, Mark Sandler, Andrew Howard, and Quoc V Le. MnasNet: Platform-Aware Neural Architecture Search for Mobile. In *CVPR*, 2019. 3
- [57] Bichen Wu, Xiaoliang Dai, Peizhao Zhang, Yanghan Wang, Fei Sun, Yiming Wu, Yuandong Tian, Peter Vajda, Yangqing Jia, and Kurt Keutzer. FBNet: Hardware-Aware Efficient ConvNet Design via Differentiable Neural Architecture Search. In *CVPR*, 2019. 3
- [58] Ji Lin, Wei-Ming Chen, Yujun Lin, John Cohn, Chuang Gan, and Song Han. Mccnet: Tiny deep learning on iot devices. In *NeurIPS*, 2020. 3
- [59] Ji Lin, Richard Zhang, Frieder Ganz, Song Han, and Jun-Yan Zhu. Anycost gans for interactive image synthesis and editing. In *CVPR*, 2021. 3
- [60] Han Shu, Yunhe Wang, Xu Jia, Kai Han, Hanting Chen, Chunjing Xu, Qi Tian, and Chang Xu. Co-evolutionary compression for unpaired image translation. In *ICCV*, 2019. 3
- [61] Yuchen Liu, Zhixin Shu, Yijun Li, Zhe Lin, Federico Perazzi, and Sun-Yuan Kung. Content-aware gan compression. In *CVPR*, 2021. 3
- [62] Ruixin Ma and Junying Lou. Cpgan: An efficient architecture designing for text-to-image generative adversarial networks based on canonical polyadic decomposition. *Scientific Programming*, 2021. 3
- [63] Angeline Aguineldo, Ping-Yeh Chiang, Alex Gain, Ameya Patil, Koltan Pearson, and Soheil Feizi. Compressing gans using knowledge distillation. *arXiv preprint arXiv:1902.00159*, 2019. 3
- [64] Song Han, Jeff Pool, John Tran, and William Dally. Learning both weights and connections for efficient neural network. *NeurIPS*, 2015. 3
- [65] Hao Li, Asim Kadav, Igor Durdanovic, Hanan Samet, and Hans Peter Graf. Pruning filters for efficient convnets. *ICLR*, 2016. 3
- [66] Baoyuan Liu, Min Wang, Hassan Foroosh, Marshall Tappen, and Marianna Pensky. Sparse convolutional neural networks. In *CVPR*, 2015. 3
- [67] Max Jaderberg, Andrea Vedaldi, and Andrew Zisserman. Speeding up convolutional neural networks with low rank expansions. In *BMVC*, 2014. 3
- [68] Haotian Tang, Zhijian Liu, Xiuyu Li, Yujun Lin, and Song Han. Torchsparse: Efficient point cloud inference engine. In *MLSys*, 2022. 3
- [69] Gernot Riegler, Ali Osman Ulusoy, and Andreas Geiger. Octnet: Learning deep 3d representations at high resolutions. In *CVPR*, 2017. 3
- [70] Mengye Ren, Andrei Pokrovsky, Bin Yang, and Raquel Urtasun. Sbnnet: Sparse blocks network for fast inference. In *CVPR*, 2018. 3, 4, 5
- [71] Patrick Judd, Alberto Delmas, Sayeh Sharify, and Andreas Moshovos. Cnvlutin2: Ineffectual-activation-and-weight-free deep neural network computing. *arXiv preprint arXiv:1705.00125*, 2017. 3
- [72] Shaohuai Shi and Xiaowen Chu. Speeding up convolutional neural networks by exploiting the sparsity of rectifier units. *arXiv preprint arXiv:1704.07724*, 2017. 3
- [73] Xuanyi Dong, Junshi Huang, Yi Yang, and Shuicheng Yan. More is less: A more complicated network with less inference complexity. In *CVPR*, 2017. 3
- [74] Bowen Pan, Wuwei Lin, Xiaolin Fang, Chaoqin Huang, Bolei Zhou, and Cewu Lu. Recurrent residual module for fast inference in videos. In *CVPR*, 2018. 3
- [75] Xiaoxiao Li, Ziwei Liu, Ping Luo, Chen Change Loy, and Xiaoou Tang. Not all pixels are equal: Difficulty-aware semantic segmentation via deep layer cascade. In *CVPR*, 2017. 3
- [76] Thomas Verelst and Tinne Tuytelaars. Dynamic convolutions: Exploiting spatial sparsity for faster inference. In *CVPR*, 2020. 3
- [77] Longguang Wang, Xiaoyu Dong, Yingqian Wang, Xinyi Ying, Zaiping Lin, Wei An, and Yulan Guo. Exploring sparsity in image super-resolution for efficient inference. In *CVPR*, 2021. 3
- [78] Yizeng Han, Gao Huang, Shiji Song, Le Yang, Yitian Zhang, and Haojun Jiang. Spatially adaptive feature refinement for efficient inference. *TIP*, 2021. 3

- [79] Yulin Wang, Yang Yue, Yuanze Lin, Haojun Jiang, Zihang Lai, Victor Kulikov, Nikita Orlov, Humphrey Shi, and Gao Huang. Adafocus v2: End-to-end training of spatial dynamic networks for video recognition. In *CVPR*, 2022. 3
- [80] Mathias Parger, Chengcheng Tang, Christopher D Twigg, Cem Keskin, Robert Wang, and Markus Steinberger. Deltacnn: End-to-end cnn inference of sparse frame differences in videos. In *CVPR*, 2022. 3
- [81] Sergey Ioffe and Christian Szegedy. Batch normalization: Accelerating deep network training by reducing internal covariate shift. In *ICML*, 2015. 5
- [82] Dmitry Ulyanov, Andrea Vedaldi, and Victor Lempitsky. Instance normalization: The missing ingredient for fast stylization. *arXiv preprint arXiv:1607.08022*, 2016. 5, 7
- [83] Xun Huang and Serge Belongie. Arbitrary style transfer in real-time with adaptive instance normalization. In *ICCV*, 2017. 5
- [84] Yuxin Wu and Kaiming He. Group normalization. In *ECCV*, 2018. 5, 7
- [85] Alexander Quinn Nichol and Prafulla Dhariwal. Improved denoising diffusion probabilistic models. In *ICML*, 2021. 5
- [86] Yaoyao Ding, Ligeng Zhu, Zhihao Jia, Gennady Pekhimenko, and Song Han. Ios: Inter-operator scheduler for cnn acceleration. *MLSys*, 2021. 5
- [87] Zhihao Jia, Oded Padon, James Thomas, Todd Warszawski, Matei Zaharia, and Alex Aiken. Taso: optimizing deep learning computation with automatic generation of graph substitutions. In *SOSP*, 2019. 5
- [88] Kaiming He, Xiangyu Zhang, Shaoqing Ren, and Jian Sun. Deep residual learning for image recognition. In *CVPR*, 2016. 5, 15
- [89] Geoffrey Hinton, Oriol Vinyals, Jeff Dean, et al. Distilling the knowledge in a neural network. *arXiv preprint arXiv:1503.02531*, 2(7), 2015. 6
- [90] Xingyi Zhou, Rohit Girdhar, Armand Joulin, Philipp Krähenbühl, and Ishan Misra. Detecting twenty-thousand classes using image-level supervision. In *arXiv preprint arXiv:2201.02605*, 2021. 6
- [91] Shengyu Zhao, Jonathan Cui, Yilun Sheng, Yue Dong, Xiao Liang, Eric I Chang, and Yan Xu. Large scale image completion via co-modulated generative adversarial networks. In *ICLR*, 2021. 6
- [92] Richard Zhang, Phillip Isola, Alexei A Efros, Eli Shechtman, and Oliver Wang. The unreasonable effectiveness of deep features as a perceptual metric. In *CVPR*, 2018. 6
- [93] Martin Heusel, Hubert Ramsauer, Thomas Unterthiner, Bernhard Nessler, and Sepp Hochreiter. Gans trained by a two time-scale update rule converge to a local nash equilibrium. *NeurIPS*, 2017. 6
- [94] Gaurav Parmar, Richard Zhang, and Jun-Yan Zhu. On aliased resizing and surprising subtleties in gan evaluation. In *CVPR*, 2022. 6
- [95] Fisher Yu, Vladlen Koltun, and Thomas Funkhouser. Dilated residual networks. In *CVPR*, 2017. 6
- [96] Sheng-Yu Wang, Oliver Wang, Richard Zhang, Andrew Owens, and Alexei A Efros. Cnn-generated images are surprisingly easy to spot... for now. In *CVPR*, 2020. 10
- [97] Han Zhang, Ian Goodfellow, Dimitris Metaxas, and Augustus Odena. Self-attention generative adversarial networks. In *ICML*, 2019. 18
- [98] Ashish Vaswani, Noam Shazeer, Niki Parmar, Jakob Uszkoreit, Llion Jones, Aidan N Gomez, Łukasz Kaiser, and Illia Polosukhin. Attention is all you need. *NeurIPS*, 2017. 18

A Kernel Fusion

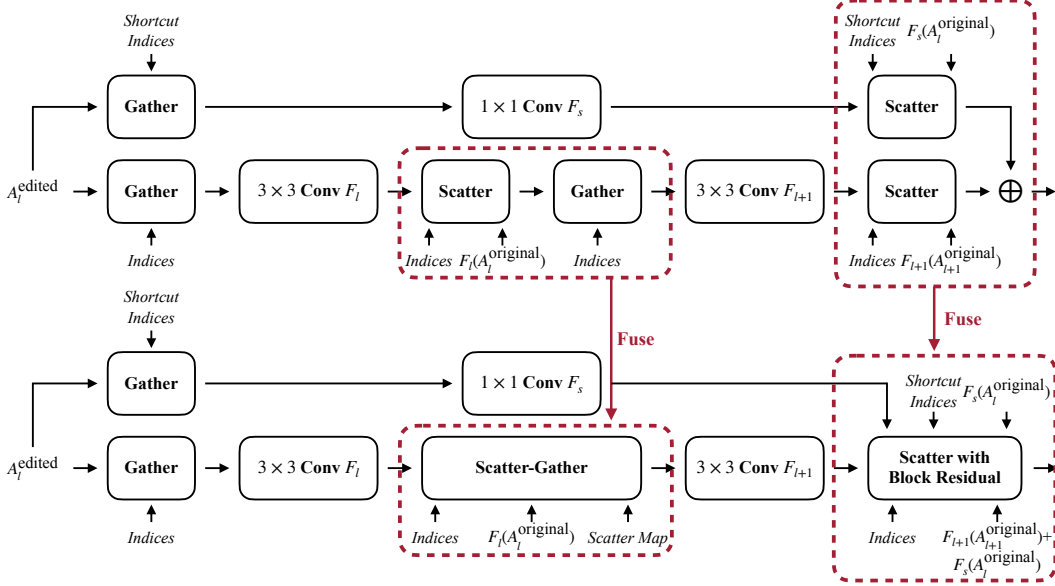


Figure 7: Visualization of kernel fusion in DDIM [5] ResBlock [88]. We omit the element-wise operations for simplicity and follow the notations in Section 3. As the kernel sizes of the convolution in the shortcut branch and main branch are different (*Indices* and *Shortcut Indices*). To reduce the tensor copying overheads in Scatter, we fuse Scatter with the following Gather into Scatter-Gather and fuse the Scatter in the shortcut, main branch, and residual addition into Scatter with Block Residual. We pre-compute an additional *Scatter Map* for the Scatter-Gather kernel.

As mentioned in Section 3.2, we fuse Scatter and the following Gather into a Scatter-Gather operator and fuse Scatter in the shortcut, main branch, and residual addition together into Scatter with Block Residual. The detailed fusion pattern is shown in Figure 7. For simplicity, we omit the element-wise operations (e.g., Nonlinearity and Scale+Shift). Below we elaborate on each fusion design. Please refer to our [code](#) for the detailed implementation.

Scatter-Gather fusion. When a Gather directly follows a Scatter, we could fuse these two operators into a Scatter-Gather to avoid copying the entire original activation $F_l(A_l^{\text{original}})$. As shown in Figure 8(a), in the original pipeline, the black blocks are copied from the original activation and then discarded by Gather, which incur redundant data movement. To address this issue, we pre-build a *Scatter Map* to track the data source (Figure 8(b)). For example, if the data at position (h, w) in the Scatter output comes from the original activation, then Scatter Map will store NULL at (h, w) (gray blocks). Otherwise, it will store a triple at this position (non-gray blocks). The first element of the triple indicates the block ID that the data come from, while the latter two indicate the offsets of the data within the block. Note that the pre-computation is cheap and only needs to be computed once for each resolution. Therefore, in the fused Scatter-Gather, we could use the Scatter Map to index and fetch the data directly from either the input blocks or the original activation, given the Gather indices. For example, if we want to fetch the data at location (h, w) , we will look up this position in the Scatter Map. If it is NULL, we would fetch the data at location (h, w) in the original activation. Otherwise, we will fetch data in the input blocks indexed by the triple. In this way, we could avoid copying the unused regions in Scatter.

Shortcut Scatter fusion. The 1×1 convolution in the shortcut branch consumes much less computation than the convolution in the main branch. Therefore the overheads of Gather and Scatter weigh more in the shortcut branch. We fuse the Scatter in the shortcut branch and main branch along with residual addition into Scatter with Block Residual to reduce these overheads. Specifically, as shown in Figure 7, we first scatter F_{l+1} output into the pre-computed $F_{l+1}(A_{l+1}^{\text{original}}) + F_s(A_l^{\text{original}})$ and add the original residual $F_s(A_l^{\text{original}})$ only at the scattered locations correspondingly according to

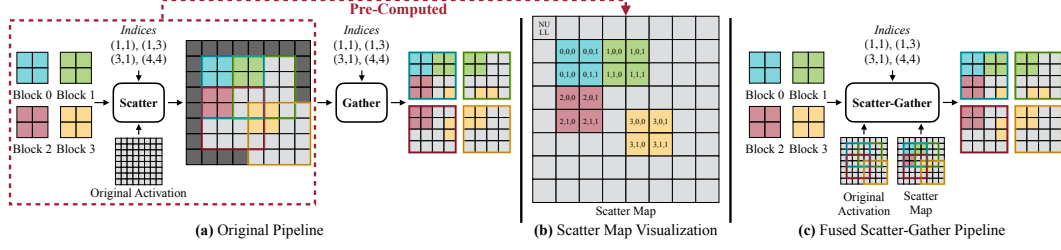


Figure 8: Scatter-Gather fusion visualization. **(a)** The original pipeline of a **Gather** directly follows a **Scatter**. The indices indicate the top left corner of the **Scatter/Gather** position (zero-based). The black blocks are discarded by the **Gather**, which incur redundant data movement. **(b)** We pre-compute the **Scatter** process and get a **Scatter Map**, which tracks the data source during **Scatter**. If the data come from the original activation, it stores **NULL** at this location (gray blocks). Otherwise, it will store a triple locating the data in the input blocks (non-gray blocks). **(c)** In the fused **Scatter-Gather** kernel, we directly use the **Scatter Map** to index and fetch the data from the input blocks and the original activation, avoiding copying the entire original feature map.

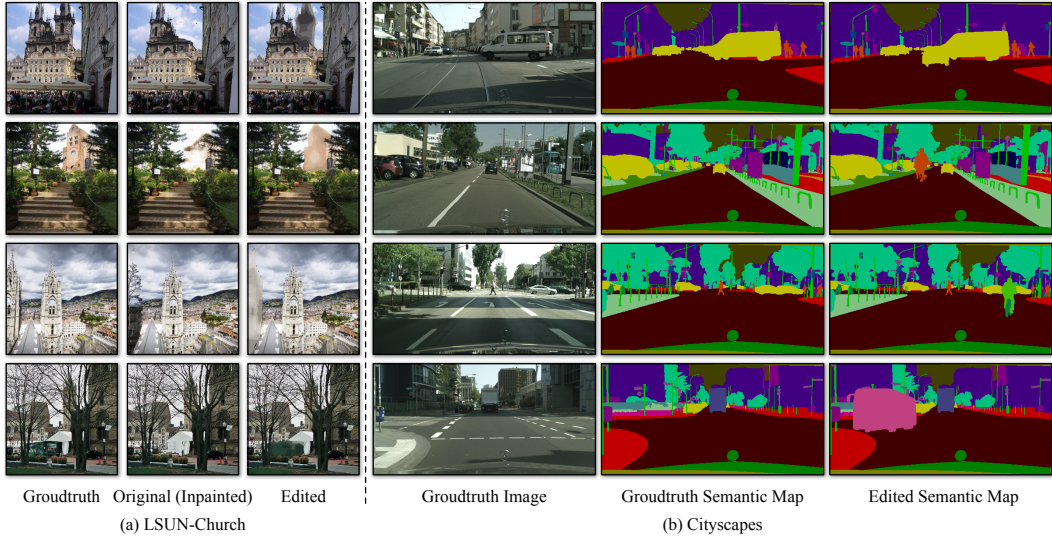


Figure 9: Examples of our synthetic edits on (a) LSUN Church and (b) Cityscapes. On LSUN Church, we view the inpainted image as the original image and generate the edits by quantizing color at the corresponding regions. On Cityscapes, we generate the edits by pasting some foreground objects on the ground-truth semantic maps.

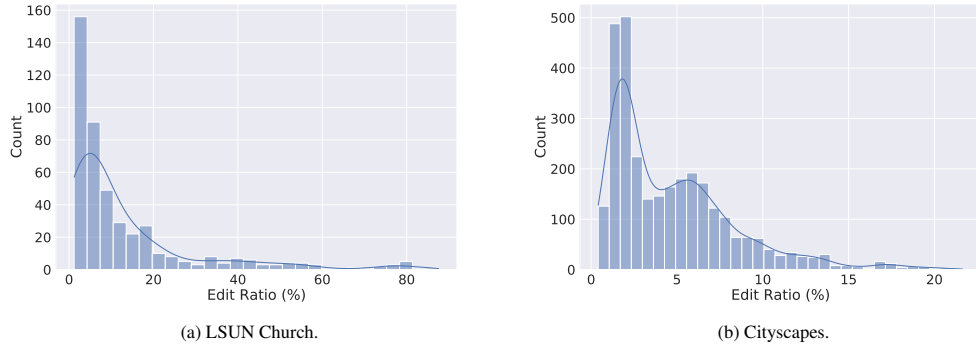


Figure 10: Detailed edit ratio distribution of our synthetic datasets.

Indices. Then we calibrate the resulting feature map with F_s output by adding the residual difference $F_s(A_l^{\text{edited}}) - F_s(A_l^{\text{original}})$ at the scattered locations indexed by *Shortcut Indices* in place.

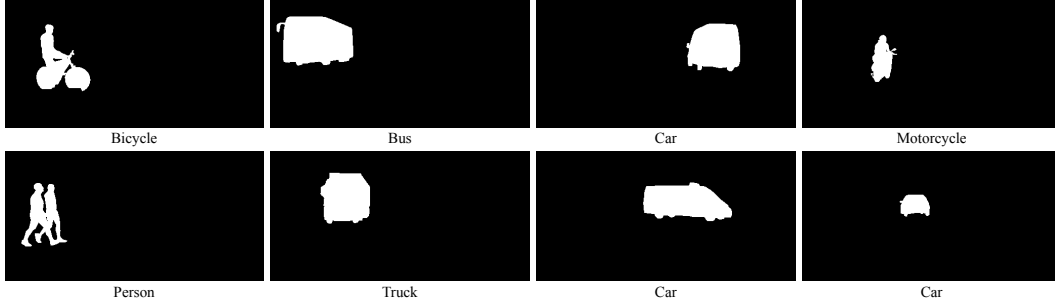


Figure 11: Several examples of our collected foreground object semantic masks.



Figure 12: Visualization results of different dilation sizes on GauGAN. Although without mIoU improvement, increasing the dilation could smoothly blend the boundary between the edited region and unedited regions to improve the image quality slightly. Specifically, the shadow boundary of the added car fades when dilation increases. However, it will incur more computations.

B Benchmark Datasets

We elaborate on how we build the synthetic edit datasets.

LSUN Church. Figure 9(a) shows some examples of our synthetic edits on LSUN Church. The average edited area of the whole dataset is 13.1%. The detailed distribution is shown in Figure 10a.

Cityscapes. We collect 27 foreground object semantic masks from the validation set. The objects include 4 bicycles, 1 motorcycle, 7 cars, 6 trucks, 3 buses, 5 persons, and 1 train. Figure 11 visualizes some collected semantic masks. We generate the edits by randomly pasting one of these objects to the ground-truth semantic maps with augmentation. The augmentation includes random horizontal flip, resize (scale factor in $[0.8, 1.2]$), and translation ($[-32, 32]$ for vertical one and $[-64, 64]$ for horizontal one). To make the synthetic edits more reasonable, when the scale factor is larger than 1, the vertical translation can only be positive. Otherwise, it can only be negative. Figure 9(b) shows some edit examples. The average edited area of the entire dataset is 4.77%. The detailed distribution is shown in Figure 10b.

C Additional Results

Dilation hyper-parameter. We show the results of our method with different dilation sizes on GauGAN in Figure 12. Increasing the dilation incurs more computations but also slightly improves the image quality. Specifically, the shadow boundary of the added car fades as the dilation increases. We choose dilation 1 since the image quality is almost the same as 20 while delivering the best speed.

Quality results at the edited regions. In Table 1, we show the quantitative quality results of our method on DDIM [5], Progressive Distillation (PD) [13] and GauGAN [8]. For DDIM and PD, the unedited regions in the generated images keep the same as the input images due to the mask trick [9]. For GauGAN, the generated unedited regions vary across different methods. In this case, the image quality at these regions will influence the metrics we report in Table 1. We additionally include the quantitative quality results of GauGAN at the sole edited regions in Table 4. Our method could still preserve the image quality of original GauGAN and match the performance of GAN Compression [10]. When applied to GAN Compression, it achieves $40\times$ MACs reduction on average, achieving results on par with *GAN Comp. (S)* with less computation.

Method	MACs		PSNR (\uparrow)		LPIPS (\downarrow)		mIoU (\uparrow)
	Value	Ratio	with G.T.	with Orig.	with G.T.	with Orig.	
Original	281G	–	15.9	–	0.414	–	57.3
GAN Comp. [10]	31.2G	9.0 \times	15.8	19.1	0.417	0.329	56.3
Ours	30.7G	9.2\times	15.9	27.5	0.425	0.076	56.1
0.19 GauGAN	13.3G	21 \times	15.4	18.4	0.427	0.356	49.5
GAN Comp. (S)	9.64G	29 \times	15.8	18.9	0.422	0.344	51.2
GAN Comp.+Ours	7.06G	40\times	15.8	18.8	0.429	0.345	52.4

Table 4: Quality evaluation of GauGAN at the edited regions. PSNR/LPIPS *with G.T.* means computing the metrics with the ground-truth images, and *with Orig.* means computing with the generated samples from the original model. *0.19 GauGAN*: Reducing each layer of GauGAN to 19% channels and training from scratch. *GAN Comp. (S)*: GAN Compression with larger compression ratio. Our method could match the performance of GAN Compression [10]. When applying it to GAN Compression, our method achieves results on par with *GAN Comp. (S)* with less computation, achieving 40 \times MACs reduction.

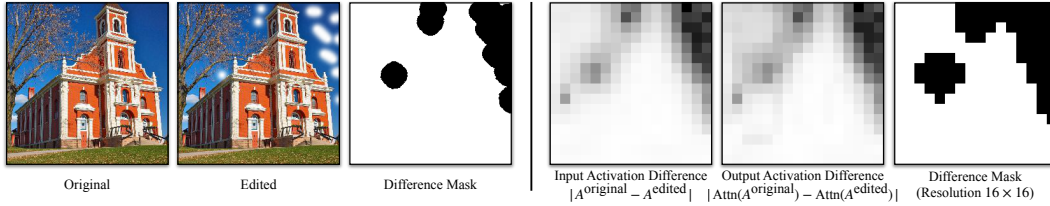


Figure 13: The input and output activation differences of a 16×16 self-attention layer in vanilla DDIM. Left: Detailed edit example with the difference mask. Right: Activation differences with the downsampled difference mask. *Attn* is the self-attention layer. Both the input difference and output difference match the difference mask very well.

Working with self-attention layers. Recent generative models often adopt attention layers to improve the generated image quality [97, 98]. Such attention layers could model long-range and multi-level dependencies across image regions, which may break the local correspondence between the edited regions in the input image and the generated images. In Figure 13, we visualize the difference between the input and output activations of a 16×16 self-attention layer in the vanilla DDIM model. The patterns of the input and output activation differences are quite similar and match the difference mask very well. This shows that the local correspondence of user edits still exists with self-attention layers, which justifies our Spatially Sparse Inference algorithm.

Large edits. In Table 5 and Figure 14, we show the results of large edits ($\sim 35\%$) using our method. Specifically, we could achieve at most $1.7\times$ speedup on DDIM, $1.5\times$ speedup on PD256 and $1.7\times$ speedup on GauGAN without losing visual fidelity. Furthermore, in many practical cases, users can decompose a large edit into several small edits. Our method could incrementally update the results instantly when the edit is being created, as described below.

Sequential edits. In Figure 15, we show the results of sequential edits with our method. Specifically, *One-time Pre-computation* performs as well as the *Full Model*, demonstrating that our method can be applied to multiple sequential edits with only one-time pre-computation in most cases. Moreover, for extremely large edits, we could use SIGE to incrementally update the pre-computed features (*Incremental Pre-computation*) and condition the later edits on the recomputed one. Its results are also as good as the full model. Therefore, our method could well address the sequential edits.

Additional visualization. In Figure 16, we show additional synthetic edit visual results of DDIM [5] and Progressive Distillation [13] on LSUN Church [11]. In Figure 17, we show additional synthetic edit visual results of GauGAN on Cityscapes [12].

Model	Edit Size	Method	MACs		3090		2080Ti		Intel Core i9-10920X		Apple M1 Pro	
			Value	Ratio	Value	Ratio	Value	Ratio	Value	Ratio	Value	Ratio
DDIM	–	Original	248G	–	37.5ms	–	54.6ms	–	609ms	–	12.9s	–
	32.9%	Ours	115G	2.2×	26.0ms	1.4×	36.9ms	1.5×	449ms	1.4×	7.53s	1.7×
PD256	–	Original	119G	–	35.1ms	–	51.2ms	–	388ms	–	6.18s	–
	32.9%	Ours	64.3G	1.9×	25.3ms	1.4×	35.1ms	1.5×	334ms	1.2×	4.47s	1.4×
GauGAN	–	Original	281G	–	45.4ms	–	49.5ms	–	682ms	–	14.1s	–
	–	GAN Compression	31.2G	9.0×	17.0ms	2.7×	25.0ms	2.0×	333ms	2.1×	2.11s	6.7×
	38.7%	Ours	148G	1.9×	27.9ms	1.6×	41.7ms	1.2×	512ms	1.3×	8.37s	1.7×
	–	GAN Comp.+Ours	18.3G	15×	15.3ms	3.0×	22.2ms	2.2×	169ms	4.0×	1.25s	11×

Table 5: Measured latency speedup of large edits on different devices. The detailed edit examples are shown in Figure 14. Our method could reduce up to 2.2× MACs, and 1.4×, 1.5×, 1.4× and 1.7× latency on NVIDIA RTX 3090, 2080Ti, Intel Core i9-10920X and M1 Pro CPU. With GAN Compression, we could further accelerate GauGAN by 4.0× on Intel Core-i9 and 11× on Apple M1 Pro CPU.

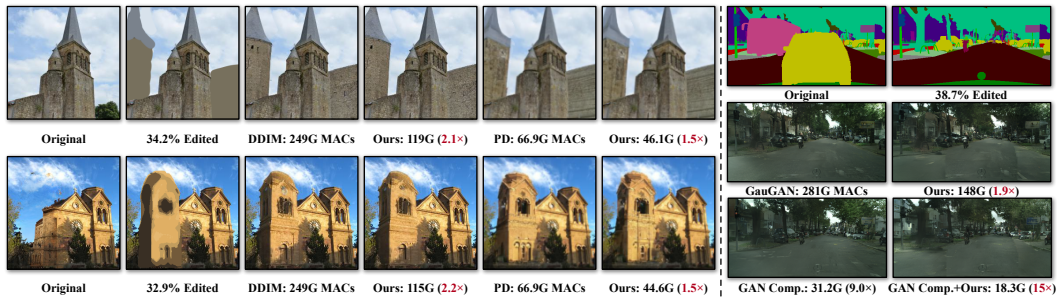


Figure 14: Qualitative results of our method with large edits. Our method could still well preserve the visual fidelity of the original model without losing global context while reducing the computation by 1.5 ~ 1.9×.

D License & Computation Resources

Here we show all the licenses of our used assets. The model **DDIM** [5], **Progressive Distillation** [13], **GauGAN** [8] and **GAN Compression** [10] is under **MIT license**, **Apache license**, **Creative Commons license** and **BSD license**, respectively. **SDEdit** is under **MIT license**. The license of Cityscapes [12] is [here](#). LSUN Church [11] does not have an explicit license.

Since our method does not involve any model training, all our generated results are obtained on a single NVIDIA RTX 3090, which only takes 1 ~ 2 hours to process all the test images (~ 7,000 in total), including both the original models and our method. We measure the model latency on NVIDIA RTX 3090, 2080Ti, Intel Core i9-10920X CPU, and Apple M1 Pro CPU. On Apple M1 Pro, we use Intel Anaconda for our Python environment.

E Changelog

V1 Initial preprint release (NeurIPS 2022).

V2 Fix the figure display issue on the cellphone.

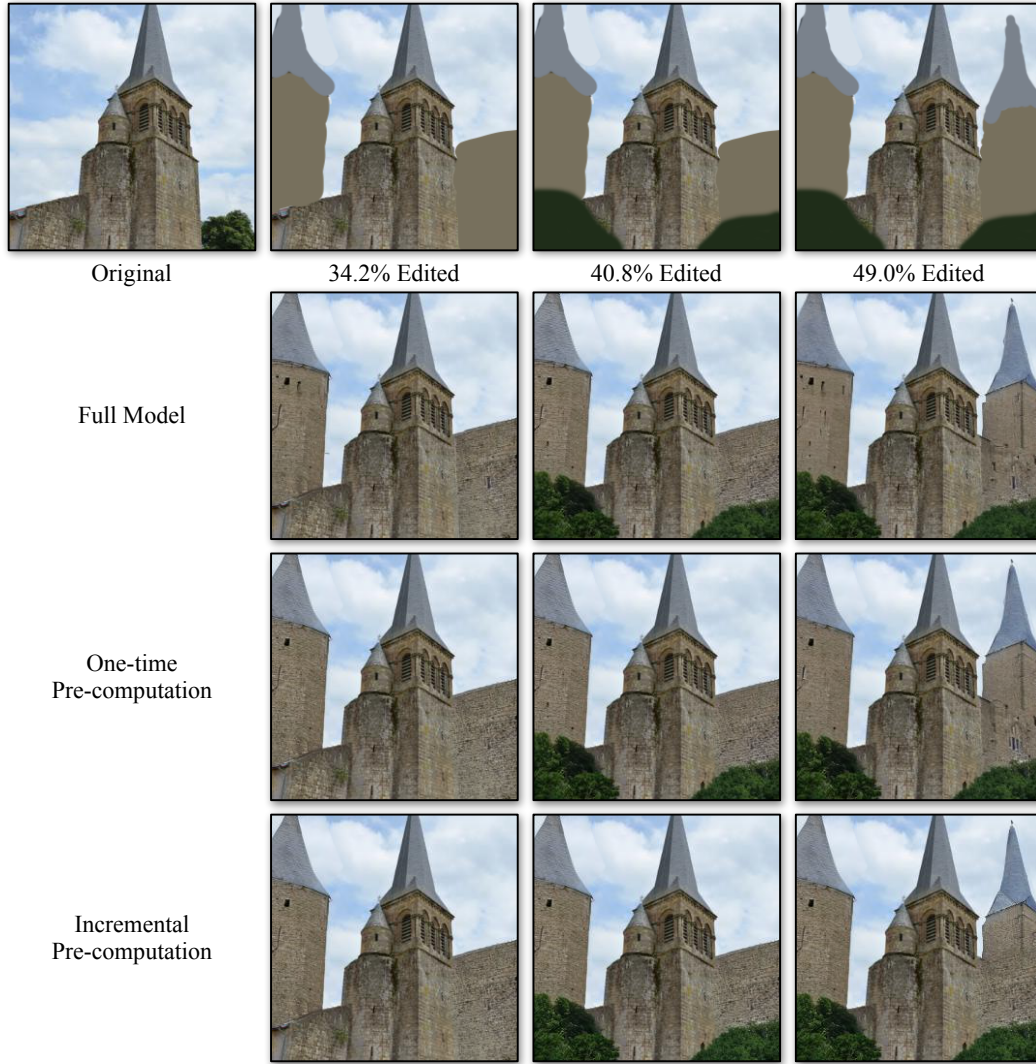


Figure 15: Sequential edit results with SIGE. *Full Model* means the results with the full model. *One-time Pre-computation* means we pre-compute the original image features for all the edit steps. *Incremental Pre-computation* means we incrementally update the pre-computed features with SIGE before the next edit step. The image quality of all methods is quite similar.

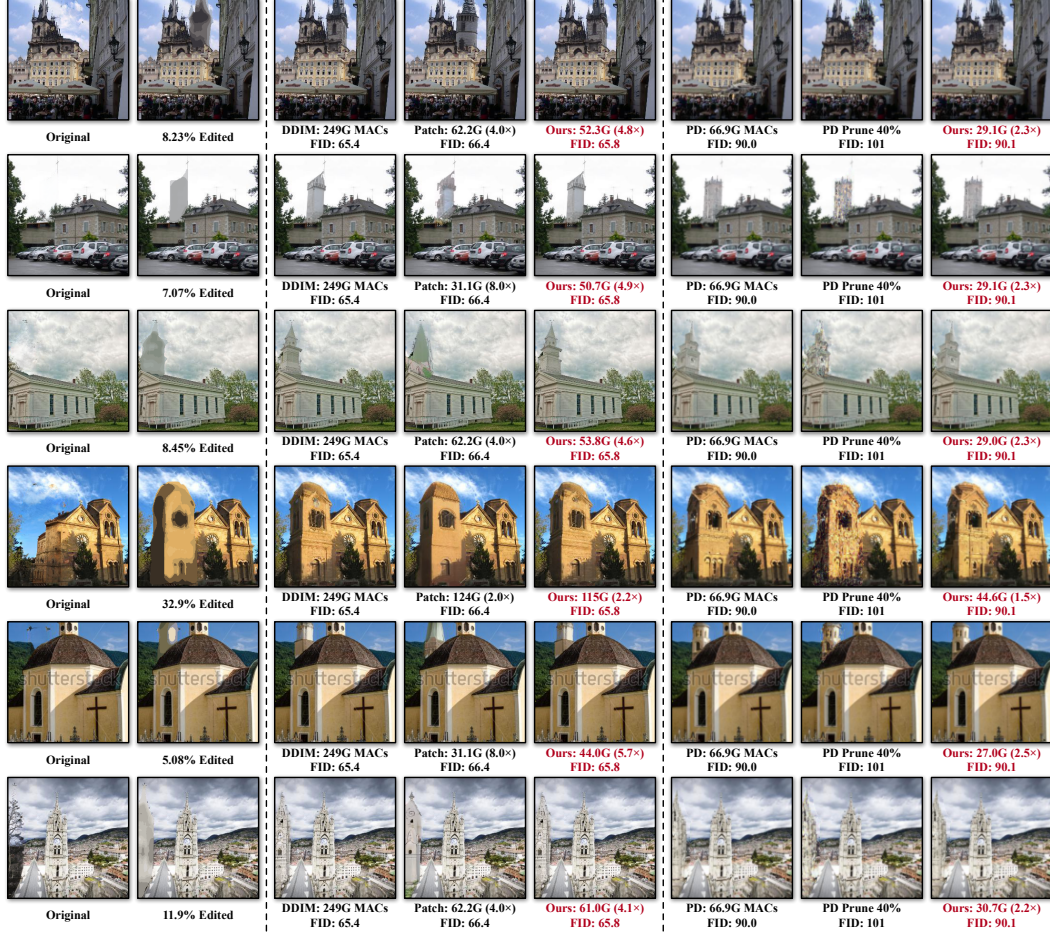


Figure 16: More visualization results on LSUN Church of DDIM [5] and Progressive Distillation. *Prune 40%*: Uniformly pruning 40% weights of the model without fine-tuning. *Patch*: Cropping the smallest image patch that covers all the edited regions of the model input and blending the model output back to the input image. Our method achieves lower FID with fewer MACs for both DDIM and progressive distillation.

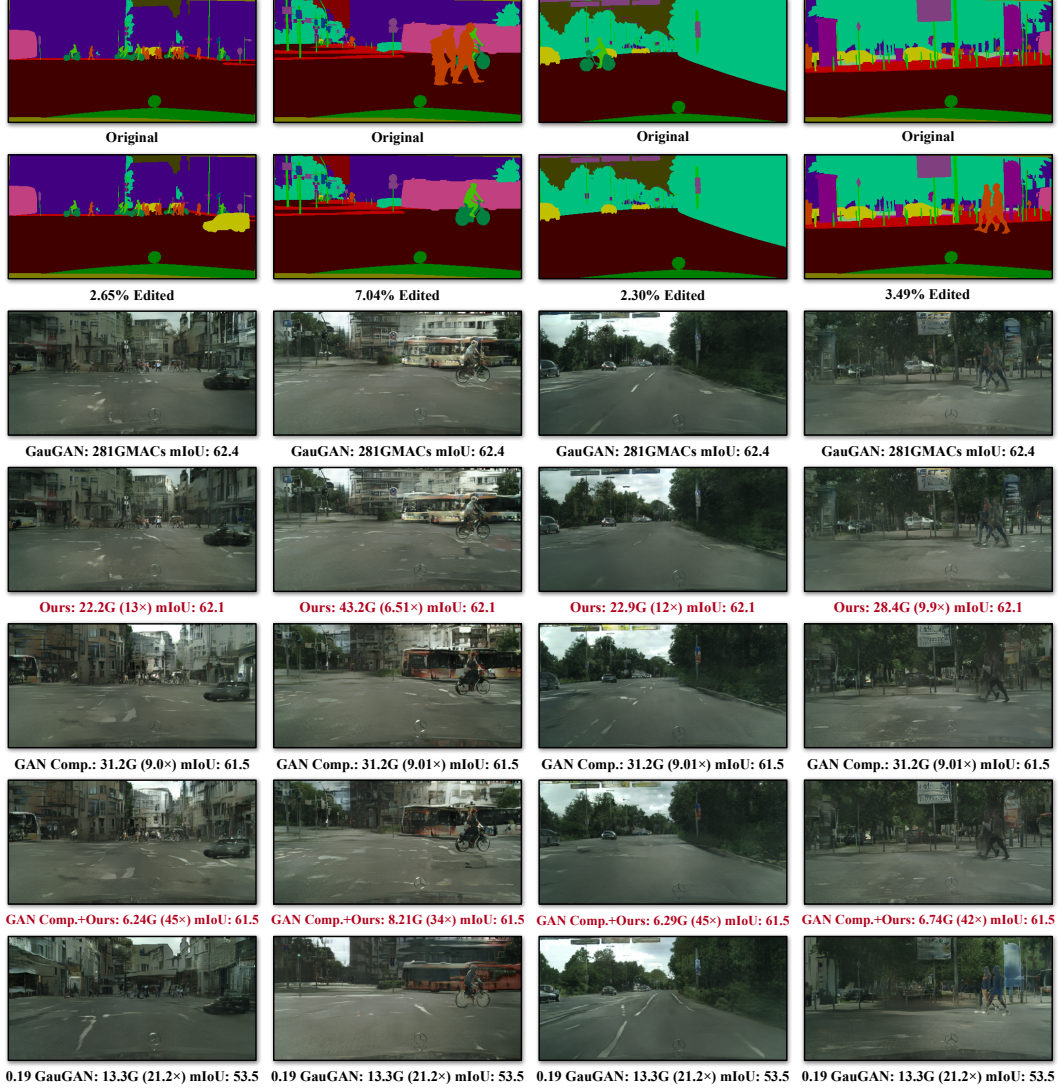


Figure 17: More visualization results on Cityscapes of GauGAN [8]. *0.19 GauGAN*: Uniformly reducing each layer of GauGAN to 19% channels and training from scratch. Our method could achieve higher mIoU than GAN Compression with fewer MACs. When applying to GAN Compression, our method achieves a 34 ~ 45× MACs reduction with a minor mIoU drop.